Available online at www.sciencedirect.com
ScienceDirect
Ceramics International 36 (2010) 1905–1910
CERAMICS INTERNATIONAL
www.elsevier.com/locate/ceramint

Characterization and X-ray peak broadening analysis in PZT nanoparticles prepared by modified sol–gel method

A. Khorsand Zak *, W.H. Abd. Majid

Solid State Laboratory, Department of Physics, University of Malaya, Kuala Lumpur 50603, Malaysia

Received 27 January 2010; received in revised form 8 February 2010; accepted 20 March 2010
Available online 15 May 2010

Abstract

Lead zirconate titanate nanoparticles (PZT-NPs) were synthesized by a modified sol–gel method and were calcinated at temperatures of 600, 650 and 700 °C. Fourier transform infrared (FTIR), powder X-ray diffraction (XRD) and thermal analysis (TGA/DTA), indicate that single-phase perovskite PZT-NPs are obtained after heat treatment at a temperature of 650 °C. The TEM results obtained from the PZT-NPs confirm that the morphology of the PZT nanoparticles is spherical, with an average diameter size of 17 nm. We also investigated the crystallite development in the nanostructured PZT by X-ray peak broadening analysis. The individual contribution of many small crystallite sizes and lattice strains to the peak broadening in the PZT nanoparticles prepared at different temperatures were studied using Williamson–Hall (W–H) analysis in the range of $2\theta = 15–80^{\circ}$.

Keywords: A. Sol–gel process; B. Grain size; B. X-ray methods; D. PZT

1. Introduction

Lead zirconate titanate ($PbZr_xTi_{1-x}O_3$ (PZT)), has been extensively used in electronic devices such as ferroelectric memories, sensors, optical fibers, shutters, actuators and modulators [1]. PZT exhibits a perovskite structure, which enhances the piezoelectric properties of the PZT at the morphotropic phase boundary (MPB) that occurs in $Pb(Zr_{0.53},Ti_{0.48})O_3$ composition[2]. It is widely accepted that the performance of PZT ceramics strongly depends on the chemical homogeneity, particle size and morphology of the starting PZT powders.

Researchers have focused on the synthesis of nano-crystalline particles. Several methods have been investigated to prepare PZT-NPs, such as hydrothermal [3,4], sol–gel combustion [5–8], sol–gel co-precipitation [9], electrohydrodynamic atomization [10,11], ultrasonic spray combustion synthesis (USCS) [12] and sol–gel [13–15]. Some of the particle sizes of PZT-NP particles prepared by some of these methods are shown in Table 1. The sol–gel method has been used to prepare single-phase nano-crystalline PZT powders, ceramics, fibers and thin films [16–20].

The crystallite size of the particles is not generally the same as the particle size due to the presence of polycrystalline aggregates [21]. The most common techniques used for the measurement of particle size (grain size) are the Brunauer–Emmett–Teller (BET), light (laser) scattering experiment, scanning electron microscopy (SEM) and TEM analysis. Lattice strain is a measure of the distribution of lattice constants arising from crystal imperfections, such as lattice dislocation. The other sources of strain are the grain boundary triple junction, contact or sinter stresses, stacking faults, coherency stresses, etc. [22]. X-ray line broadening is used to investigate the dislocation distribution. Crystallite size and lattice strain affect the Bragg peak in different ways. Both of these effects increase the peak width and the intensity of the peak, and shift the 2θ peak position accordingly. This difference in behavior as a function of 2θ enables one to discriminate between the size and strain effect on the peak broadening. The Bragg width contribution from crystallite size is inversely proportional to the crystallite size. Williamson–Hall (W–H) analysis is a simplified integral breadth method where both, size induced and strain-induced broadening are deconvoluted by considering the peak width as a function of 2θ. Although the X-ray profile analysis is

* Corresponding author. Tel.: +60 12 2850849; fax: +60 37 9674146.
E-mail address: alikhorsandzak@gmail.com (A. Khorsand Zak).

0272-8842/$36.00
doi:10.1016/j.ceramint.2010.03.022

Table 1
Particle sizes of PZT-NP particles prepared by different methods.

Method	Size (nm)	Ref.
Hydrothermal	5–10	[3]
Electrohydrothermal	10	[11]
Sol–gel	15	[31]
Sol–gel (TEA agent)	15	[4]
Sol–gel co-precipitation	10–30	[9]
Sol–gel	35	[16]
Sol–gel combustion	78	[27]
Sol–gel auto combustion	70–110	[6]
(USCS)	100–200	[12]
Ultrasonic atomization	450	[10]

an average method, it can be used in an unavoidable position to determine grain size beside TEM micrographs [23].

In the present research, the rhombohedral free standing PZT-NPs were prepared by a simple modified sol–gel method in a polymeric system. This method is used to control nanostructure materials on the molecular scale because individual metal ions can be reduced by growing polymer nets. The segregation of particular metals was reduced by the immobilization of metal complexes, thus ensuring compositional homogeneity on a molecular scale. In addition, a comparative evaluation of the mean particle size of PZT-NPs obtained from direct TEM measurements and from powder XRD procedures is reported. The strain of PZT-NPs was estimated by a modified form of W–H, method which is the uniform deformation model, UDM. This model can be used to prepare nanoparticles on large scales for industrial purposes.

2. Experimental

Lead acetate trihydrate ($Pb(CH_3COO)_2{\cdot}3H_2O$, Merck), titanium isopropoxide ($Ti(OCH(CH_3)_2)_4$, Merck), zirconium n-propoxide ($Zr(OCH_2CH_2CH_3)_4$, 70% in L-propanol, Sigma–Aldrich), and 2-methoxyethanol ($CH_3OC_2H_4OH$, Merck) were used as the starting materials to prepare the precursor solutions for PZT-NP drawing. The atomic ratio of the Pb:Zr:Ti of the solution was 1:0.52:0.48 and 10% excess lead acetate was introduced.

Initially, 11.65 grams lead acetate was dissolved in 50 ml 2-methoxyethanol and stirred for 1 h at room temperature. Simultaneously, 7.2 ml zirconium n-propoxide was dissolved in 80 ml 2-methoxyethanol and stirred for 30 min at room temperature. Subsequently, 4.4 ml titanium isopropoxide was added to this solution and a small measure of solvent was added to the solution to reach 100 ml in total. Then it was stirred for 30 min at room temperature for the second time. The high sensitivity of titanium isopropoxide and zirconium n-propoxide to oxygen requires the solutions to be prepared in a glove box with an Argon atmosphere. While stirring the zirconium–titanium solution, lead solution was added to the solution and stirring was continuously carried out for 30 min at 60 °C temperature. The PH of the solution was adjusted to 5 by adding a small amount of pure water. After about 3 min, the color of the solution changed from clear to milky and the state of the solution changed from liquid to gelatinous. The white gel was dried at 60 °C for 2 days. Finally, the white dried gel was milled and calcinated at 600, 650 and 700 °C with a heating rate of 5 °C/min for 1 h to completely burn out the organic compounds and obtain yellow PZT-NPs. Thermogravimetric analysis (TGA) and differential thermal analysis (DTA) were used to analyze the thermal behavior and reaction mechanisms of the gel powders. The molecular structures of the solid phase were investigated by Fourier transform infrared (FTIR). The structure evolution of the PZT-NPs was studied by X-ray powder diffraction analysis (XRD). The gel preparation of PZT-NPs is shown in Fig. 1.

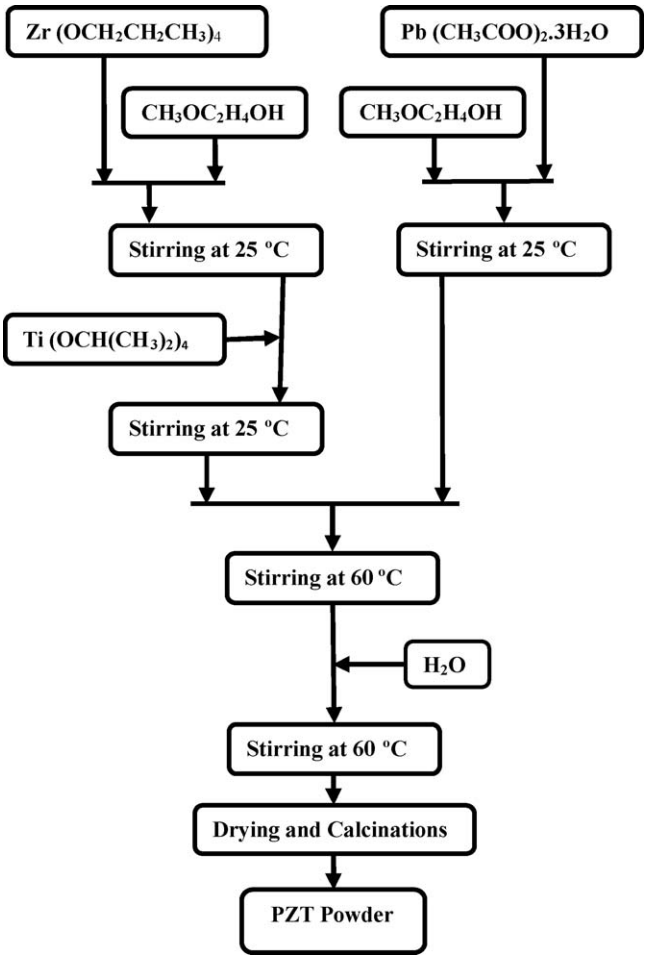

Fig. 1. Flowchart of synthesis of PZT-NPs by sol–gel method.

3. Results and discussion

3.1. Thermal analysis (TGA–DTA)

Fig. 2 shows the results of thermogravimetric analysis, TGA, and differential thermal analysis, DTA. The TG curve descends until a horizontal is obtained around 620 °C. The horizontal curve obviously corresponds to the existence of PZT. The TG and DTA traces show three main regions. The first is an initial loss of water at around 60 °C, bend Ed_1, endothermic reaction, and corresponding 4.7% weight loss. Then the decomposition

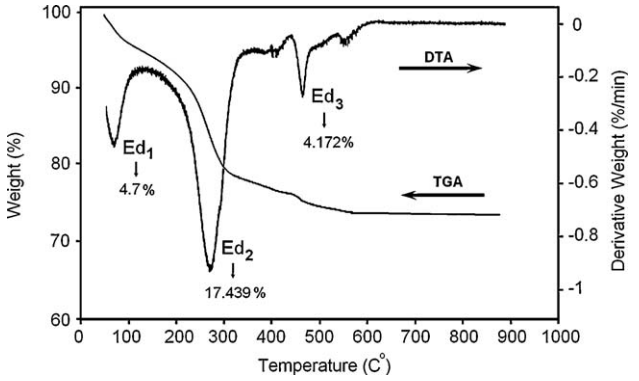

Fig. 2. Thermal gravity and derivation analysis (TGA–DTA) of dried gel of PZT.

of organic material occurs between 100 and 320 °C which corresponds to bend Ed_2, accompanied by a 17.439% weight loss. Also, this important deflection at Ed_2, whose maximum is around 260 °C, is attributed to the formation of the pyrochlore phase and the initiation of crystallization of materials. Finally, the third deflection Ed_3 that occurs around 450 °C is related to the formation of the perovskite structure of PZT-NPs accompanied by 4.172% weight loss [24]. The horizontal curves of TG\DTA are achieved around 620 °C, which indicates that the complete formation of the perovskite PZT-NPs is achieved at a furnace temperature of greater than 620 °C. The X-ray diffraction indicates that the perovskite structures are formed at around 650 °C, which agrees well with the TG\DTA results.

3.2. FTIR spectrum analysis

FTIR spectroscopy was used to study the transformation of basic material solutions during the thermal reactions, which leads to the perovskite PZT-NPs. The FTIR spectroscopy (in the range of 4000–280 cm^{-1}) of the PZT-NPs calcinated for 1 h at different temperatures of 600, 650 and 700 °C are presented in Fig. 3. As in the case of other ABO_3-type perovskite compounds, a broad band is observed for each spectrum from about 750 to 400 cm^{-1}, and another band from 400 to 300 cm^{-1}. These bands are related to B–O vibrations (BO_6 and B–O for ABO_3 structures). These results confirm the formation of the pure perovskite structure of PZT-NPs at 700 °C [25].

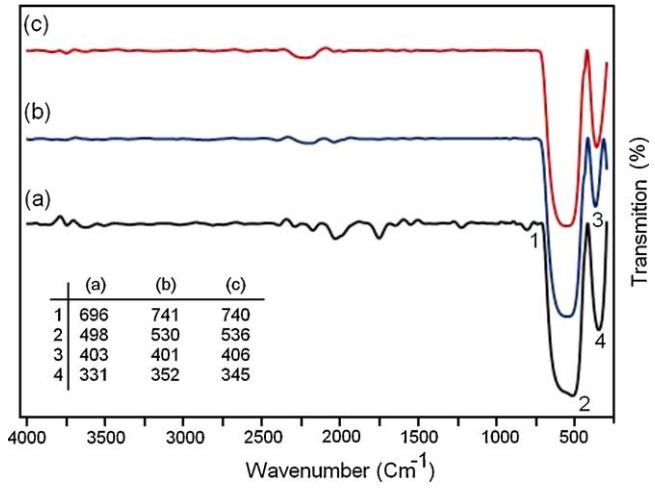

Fig. 3. FTIR spectra of prepared PZT-NPs at different calcination temperatures for 1 h: 600 °C (a), 650 °C (b) and 700 °C (c).

3.3. X-ray diffraction analysis and phase evaluation

XRD patterns of PZT-NPs annealed for 1 h at different temperatures (600, 650 and 700 °C) are shown in Fig. 4. At an annealing temperature of 600 °C, the PZT-NPs are predominantly in the rhombohedral phase, and there is also some pyrochlore phase. The rhombohedral phases are enhanced by increasing the annealing temperature to 650 °C, but at this stage a small amount of pyrochlore phase appears. At the annealing temperature of 700 °C, the pyrochlore phase disappears, while the pure rhombohedral phase is observed. The XRD results also reveal the existence of a perovskite-type phase for the PZT-NPs prepared by the sol–gel method for all temperatures. This result agrees well with the DTA measurement, which shows that the crystallization process is completed at about 650 °C. The values of, the distance d between adjacent planes in the $(h\,k\,l)$ are calculated from the Bragg equation $\lambda = 2d \sin\theta$; the lattice constants a, b, c, the interplanar angle, the angle φ between the plane $(h_1\,k_1\,l_1)$, of spacing d_1, and the plane $(h_2\,k_2\,l_2)$, of spacing d_2, and the cell volumes are calculated from the *Lattice Geometry* equation [26]. The lattice parameters of powders calcinated at different temperature are summarized in Table 2.

3.4. Particle size

The average particle size of PZT-NPs is determined by means of the X-ray line broadening method using the Scherrer equation: $D = (k\lambda/B_{hkl}\cos\theta)$, where D is the particle size in

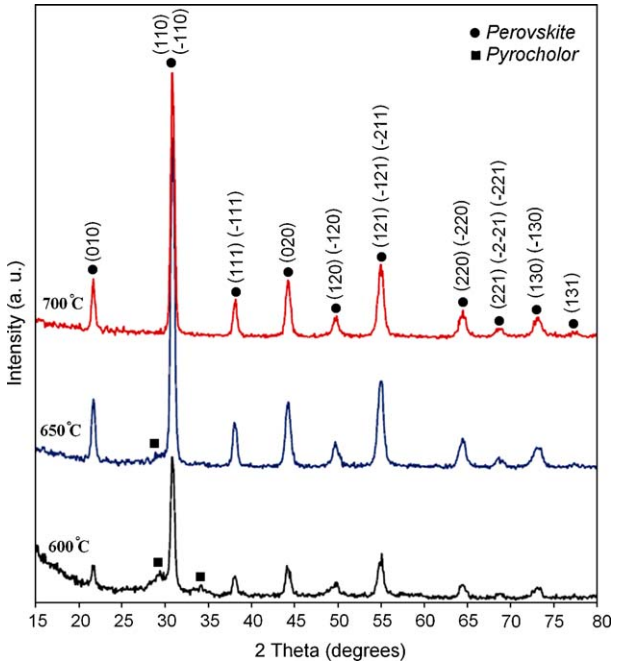

Fig. 4. XRD patterns of prepared PZT-NPs at different calcination temperatures.

Table 2
Lattice parameters of PZT-NPs prepared at different temperatures of 600, 650 and 700 °C for 1 h.

Temperature (°C)	2θ	d_{hkl} (nm)	hkl	Structure	Lattice parameter (nm)	V	cos φ
600	21.69 30.8	0.40944 0.29007	0 1 0 −1 1 0	Rhombohedral	$a = b = c = 0.40406$ $\alpha = 90.21766$	65.96496	0.730289
650	21.7 30.87	0.40952 0.28939	0 1 0 −1 1 0	Rhombohedral	a = b = $c = 0.40918$ $\alpha = 90.00280$	68.50948	0.707400
700	21.67 30.87	0.40981 0.28939	0 1 0 −1 1 0	Rhombohedral	$a = b = c = 0.41370$ $\alpha = 89.84552$	70.80841	0.691075

nanometer, λ is the wavelength of the radiation (1.5406 Å for Cu Kα radiation), k is a constant equal to 0.94, B_{hkl} is the peak width at half-maximum intensity and θ is the peak position; (1 1 0) peak is used for the rhombohedral specimen lines [27]. It is observed that the average particle size increases as the calcination temperature increases. The average particle size is found about 14 ± 2 nm, for a sample calcinated at 700 °C and free of pyrochlore phase. A summary of the average sizes of PZT-NPs calcinated at different temperatures is shown in Table 3.

The typical TEM image of PZT-NPs calcinated at a temperature of 650 °C is shown in Fig. 5. The figure shows that the PZT-NPs exhibit a narrow distribution and are almost spherical in shape. From TEM analysis, the primary particle size of PZT-NPs is found to be approximately 17 nm in diameter.

3.5. The X-ray peak broadening analysis

XRD can be utilized to evaluate the peak broadening in terms of the crystallite size and the lattice strain due to dislocation [28]. The breadth of the Bragg peak is a combination of both instrument and sample dependent effects. In order to decouple these contributions, it is necessary to collect a diffraction pattern from the line broadening of a standard material such as silicon, to determine the instrumental broadening [29]. The instrumental corrected broadening [30] B_{hkl} corresponding to the diffraction peak of PZT-NPs were estimated by using the relation:

$$B_{hkl} = \sqrt{[(B_{hkl})^2_{\text{measured}} - B^2_{\text{Instrumental}}]} \quad (1)$$

Strain-induced broadening arising from crystal imperfection and distortion were related by $\varepsilon = B_{hkl}/\tan\theta$. From this equation and the Scherrer equation, it is clear that the peak width from crystallite size varies as $1/\cos\theta$, whereas the strain varies as $\tan\theta$. Williamson and Hall (W–H) proposed a method of deconvoluting size and strain broadening by looking at the peak width as a function of the diffracting angle 2θ and obtained the mathematical expression:

$$B_{hkl} = \left(\frac{k\lambda}{D\cos\theta}\right) + 4\varepsilon\tan\theta \quad (2)$$

Rearranging Eq. (2) gives

$$B_{hkl}\cos\theta = \left(\frac{k\lambda}{D}\right) + 4\varepsilon\sin\theta \quad (3)$$

A plot is drawn with $4\sin\theta$ along the x-axis and $B_{hkl}\cos\theta$ along the y-axis for PZT-NPs calcinated at different temperatures. For the entire experiment, the plot is drawn only for the preferred orientation peaks of PZT with the rhombohedral phase. The lattice planes corresponding to those preferred peaks are (0 1 0), (1 1 0), (1 1 1), (0 2 0), (1 2 0), (1 2 1), (2 2 0), (2 2 1) and (1 3 0). From the linear fit to the data, the crystallite size D was extracted from the y-intercept and the strain ε from the slope of the fit. Eq. (3) represents the uniform

Table 3
The diameter size of PZT-NPs obtained from different methods.

Temperature (°C)	2θ (°)	FWHM (rad)	Size (nm)	Average size (nm)
600	30.870 44.176	0.533 0.721	14.78 12.42	13.6 ± 2
650	30.874 44.229	0.550 0.697	15.64 12.85	14.25 ± 2
700	30.874 44.242	0.528 0.680	16.30 13.17	14.74 ± 2

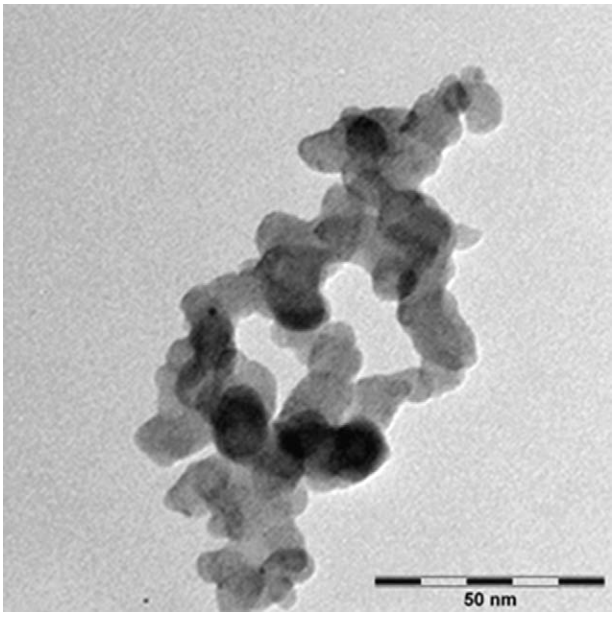

Fig. 5. TEM micrograph of the prepared PZT-NPs at calcination temperatures of 650 °C for 1 h.

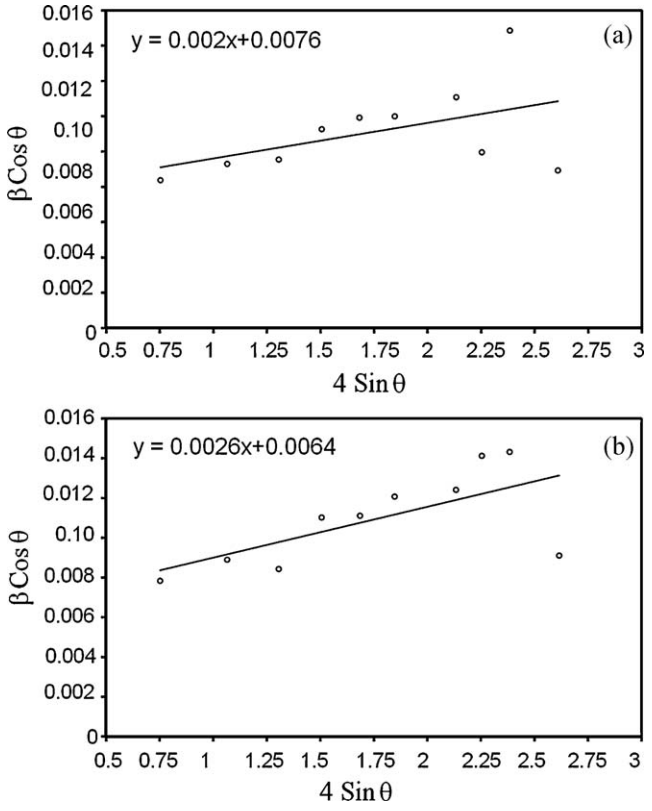

Fig. 6. The W–H analysis of PZT-NPs: $T = 650$ °C (a) and $T = 700$ °C (b).

Table 4
The W–H analysis results of PZT-NPs.

Temperature (°C)	W–H method	
	D (nm)	ε (no unit)
650	18.23	0.0020
700	21.66	0.0026

deformation model, UDM, where the strain was assumed to be uniform in all crystallographic directions, considering the isotropic nature of the crystal, where all the material properties are independent of the direction along which they are measured. The UDM for PZT-NPs calcinated at 650 and 700 °C are shown in Fig. 6 and summarized in Table 4. From this plot, it is clear that the strain and particle size of PZT-NPs calcinated at 650 °C are less than the strain and particle size of PZT-NPs calcinated at 700 °C.

4. Conclusions

Pure PZT nanoparticles were synthesized by a modified sol–gel process and characterized by powder XRD, TEM, TGA\DTA and FTIR. The XRD and FTIR patterns indicated that the perovskite PZT-NPs were free of the pyrochlore phase at 700 °C. The line broadening of PZT-NPs calcinated at 650 and 700 °C due to small crystallite size and lattice strain were analyzed by the Scherer formula and modified forms of W–H analysis. A modified W–H was analyzed and used to determine the crystallite size and strain-induced broadening. The TEM image of PZT-NPs calcinated at 650 °C reveals the average particle size of about 17 nm. The result of TEM is in good agreement with the particle size obtained from the W–H method.

Acknowledgement

This work was supported by the University of Malaya through grant No: PS 217/2009 A.

References

[1] C. Buchanan, Ceramic Materials for Electronics, Marcel Dekker, New York, 1991, 182 pp..
[2] B. Jaffe, W.R. Cook, H. Jaffe, Piezoelectric Ceramics, Academic Press Inc., New York, 1971.
[3] A.T. Chien, J. Sachleben, J.H. Kim, J.S. Speck, F.F. Lange, Synthesis and characterization of $PbTiO_3$ powders and heteroepitaxial thin films by hydrothermal synthesis, J. Mater. Res. 14 (1999) 3303–3311.
[4] Y. Deng, L. Liu, Y. Cheng, C.W. Nan, S.J. Zhao, Hydrothermal synthesis and characterization of nanocrystalline PZT powders, Mater. Lett. 57 (2003) 1675–1678.
[5] M. Cernea, G. Montanari, C. Galassi, A.L. Costa, Synthesis of La and Nb doped PZT powder by the gel-combustion method, Nanotechnology 17 (2006) 1731–1735.
[6] A. Banerjee, S. Bose, Low-temperature synthesis and densification, Chem. Mater. 16 (2004) 5610–5615.
[7] J. Schafer, W. Sigmund, S. Roy, F. Aldinger, Low temperature synthesis of ultrafine $Pb(Zr,Ti)O_3$ powder by sol–gel combustion, J. Mater. Res. 12 (1997) 2518–2521.
[8] N.S. Gajbhiye, P.K. Pandey, P. Smitha, Low-temperature synthesis of nanostructured PZT for dielectric studies, Synth. React. Inorg. Met.-Org. Nano-Met. Chem. 37 (2007) 431–435.
[9] C. Liu, B. Zou, A.J. Rondinine, Z.J. Zhang, Sol–gel synthesis of free-standing ferroelectric lead zirconate titanate nanoparticle, J. Am. Chem. Soc. 123 (2001) 4344–4345.
[10] Z.J. Xu, R.Q. Chu, G.R. Li, X. Shao, Q.R. Yin, Preparation of PZT powder and ceramics via a hybrid method of sol–gel and ultrasonic atomization, Mater. Sci. Eng. B 117 (2005) 113–118.
[11] S.N. Jayasinghe, R.A. Dorey, M.J. Edirisinghe, Z.B. Luklinska, Preparation of lead zirconate titanate nano-powder by electrohydrodynamic atomization, Appl. Phys. A 80 (2005) 723–725.
[12] S. Lee, B. Jn, Preparation of ultrafine PZT powders by ultrasonic spray combustion synthesis (USCS), Ceram. Int. 31 (2005) 53–56.
[13] Y.F. Chen, R. Nass, S. Vilminot, Seeding effects in the sol–gel preparation of lead zirconate titanate (PZT) powders, J. Sol–Gel Sci. Technol. 8 (1997) 385–389.
[14] M. Stefanescu, M. Stoia, O. Stefanescu, Thermal and FT-IR study of the hybrid ethylene–glycol–silica matrix, J. Sol–Gel Technol. 41 (2007) 71–78.
[15] Y. Fahmi, M. Shoaib, Sol–gel processing and characterization of phase-pure lead zirconate titanate nano-powders, J. Am. Ceram. Soc. 89 (2006) 2034–2037.
[16] Q.F. Zhou, H.L.W. Chen, C.L. Choy, Nanocrystalline powder and fibers of lead zirconate titanate prepared by sol–gel process, J. Mater. Process. Technol. 63 (1997) 281–285.
[17] C.Y. Lee, N.H. Tai, S.H. Hsieh, Synthesis of nano-sized polycrystalline PZT powder using molecular building blocks by designed chemical route, J. Nanoparticle Res. 8 (2006) 287–292.
[18] D.G. Wang, C.Z. Chen, J. Ma, T.H. Liu, Lead-based titanate ferroelectric thin films fabricated by a sol–gel technique, Appl. Surf. Sci. 255 (2008) 1637–1645.
[19] M. Zhang, I.M.M. Salvado, P.M. Vilarinho, Synthesis and characterization of lead zirconate titanate fibers prepared by the sol–gel method: the role of the acid, J. Am. Ceram. Soc. 86 (2003) 775–781.

[20] T.I. Chang, S.C. Wang, C.P. Liu, C.F. Liu, J.L. Huang, Thermal behaviors and phase evolution of lead zirconate titanate prepared by sol–gel processing: the role of the pyrolysis time before calcination, J. Am. Ceram. Soc. 91 (2008) 2545–2552.
[21] K. Ramakanth, Basics of X-ray Diffraction and its Application, I.K. International Publishing House PVt. Ltd., New Delhi, 2007.
[22] T. Ungar, Characterization of nanocrystalline materials by X-ray line profile analysis, J. Mater. Sci. 42 (2007) 1584–1593.
[23] R. Yogamalar, R. Srinivasan, A. Vinu, K. Ariga, A.C. Bose, X-ray peak broadening analysis in ZnO nanoparticles, Solid State Commun. 149 (2009) 1919–1923.
[24] R. Bel Hadj Taher, N. Bel Hadj Taher, A. Ben Saleh, Low-temperature processing and characterization of single-phase PZT powder by sol–gel method, J. Mater. Sci. 42 (2007) 9801–9806.
[25] J.T. Last, Infrared-absorption studies on barium titanate and related materials, Phys. Rev. 105 (1957) 1740–1750.
[26] B.D. Cullity, Elements of X-ray Diffraction, Addison–Wesley Publishing Company Inc., California, 1956.
[27] M. Ghafemifard, S.M. Hosseini, A. Khorsand Zak, G.H.H. Khorrami, Microstructure and optical characterization of PZT nanopowder prepared at low temperature, Physica E 41 (2009) 418–422.
[28] V.A. Drits, D.D. Eberl, J. Srodon, XRD measurement of mean thickness, thickness distribution and strain for illite and illite–smectite crystallites by the Bertaut–Warren–Averbach technique, Clays Clay Miner. 46 (1) (1998) 38–50.
[29] J.S. Lee, R.J. De Angelis, X-ray diffraction patterns from nanocrystalline binary alloys, Nanostruct. Mater. 7 (1996) 805–812.
[30] V. Biju, S. Neena, V. Vrinda, S.L. Salini, Estimation of lattice strain in nanocrystalline silver from X-ray diffraction line broadening, J. Mater. Sci. 43 (2008) 1175–1179.
[31] A.L. Fernandez-Osorio, A. Vazquez-Olmos, E. Mata-Zamora, J.M. Saniger, preparation of free-standing $Pb(Zr_{0.52}Ti_{0.48})O_3$ nanoparticles bye sol–gel method, J. Sol–Gel Sci. Technol. 42 (2007) 145–149.